Contemporary Chemistry

RESEARCH ARTICLE

Molecular Reactivity of some Maillard Reaction Products Studied through Conceptual DFT

Daniel Glossman-Mitnik[1]* and Juan Frau[2]

[1]Department of Environment and Energy, Centro de Investigación en Materiales Avanzados Chihuahua, Mexico
[2]Department of Chemistry, University of the Balearic Islands, Spain

Abstract

Ten density functionals that include CAM-B3LYP, LC-wPBE, M11, M11L, MN12L, MN12SX, N12, N12SX, wB97X and WB97XD in connection with the Def2TZVP basis set and the SMD solvation model (water as a solvent) have been assessed for the calculation of the molecular structure and properties of seven key chromophores formed by nonenzymatic browning of hexoses and L-alanine. The chemical reactivity descriptors for the systems are calculated via the Conceptual Density Functional Theory. The choice of active sites applicable to nucleophilic, electrophilic as well as radical attacks is made by linking them with Fukui functions indices, electrophilic Parr functions, and condensed dual descriptor Δf(r). The study found the MN12SX and N12SX density functionals to be the most appropriate in predicting the chemical reactivity of this molecule.

Keywords: Key chromophores; Conceptual DFT; Chemical reactivity; Colored maillard reaction Products; Parr functions; Dual descriptor

Introduction

As pointed out by Rizzi [1] "Visual color in processed foods is largely due to colored products of Maillard or nonenzymic browning reactions. In spite of the longstanding aesthetic and practical interest in Maillard derived food coloring materials, relatively little is known about the chemical structures responsible for visual color". These chemical structures are known as Colored Maillard Reaction Products and can be isolated at intermediate stages during the melanoidin formation process. Besides their interest as dye molecules which may be useful as food additives, but also as dyes for dye-sensitized solar cells (DSSC), these compounds have also antioxidant capabilities. Thus, they are amenable to be studied by analyzing their molecular reactivity properties. Some of these isolated molecules are called key chromophores which are formed by nonenzymatic browning of hexoses and L-alanine [2], and we believe that it could be of interest to study their molecular reactivity by using the ideas of Conceptual DFT, in the same way of our previous works [3-33]. Thus, in this computational study we will assess ten density functionals in calculating the molecular properties and structures of the seven key chromophores. Following the same ideas of previous works, we will consider fixed RSH functional instead of the optimally-tuned RSH density functionals that have attained great success [34-53].

Theoretical Background

The theoretical background of this study is similar to the previous con- ducted research presented [3-33], and will be shown here for complete purposes, because this research is a component of a major project that it is in progress. If we consider the KID procedure presented in our previous works [3-33] together with a finite difference approximation, then the global reactivity descriptors can be written as:

Electronegativity	$X = -1/2(I+A) \approx 1/2(\varepsilon_L+\varepsilon_H)$	[54,55]
Global Hardness	$\eta = (I-A) \approx (\varepsilon_L-\varepsilon_H)$	[54,55]
Electrophilicity	$\omega = \chi^2/2\eta = (I+A)^2/(4(I-A)) \approx (\varepsilon_L+\varepsilon_H)^2/(4(\varepsilon_L-\varepsilon_H))$	[56]
Electrodonating Power	$\omega^- = (3I+A)^2/(16(I-A)) \approx (3\varepsilon_H+\varepsilon_L)^2/16\eta$	[57]
Electroaccepting Power	$\omega^+ = (I+3A)^2/(16(I-A)) \approx (\varepsilon_H+3\varepsilon_L)^2/16\eta$	[57]
Net Electrophilicity	$\Delta\omega^{\pm} = \omega^+ - (-\omega^-) = \omega^+ + \omega^-$	[58]

where ε_H and ε_L are the energies of the highest occupied and the lowest unoccupied molecular orbitals (HOMO and LUMO), respectively.

Applying the same ideas, the definitions for the local reactivity descriptors are:

Correspondence to: Glossman-Mitnik D, Department of Environment and Energy, Centro de Investigación en Materiales Avanzados Chihuahua, Mexico. Email: Daniel[DOT]glossman[At]cimav[DOT]edu[DOT]mx

Received: Feb 19, 2018; **Accepted:** Feb 21, 2018; **Published:** Feb 23, 2018

Nucleophilic Fukui Function	$f^+(r) = \rho_{N+1}(r) - \rho_N(r)$	[54]
Electrophilic Fukui Function	$f^-(r) = \rho_N(r) - \rho_{N-1}(r)$	[54]
Dual Descriptor	$\Delta f(r) = (\partial f(r)/\partial N)_{v(r)}$	[59-65]
Nucleophilic Parr function	$P^-(r) = \rho_s^{rc}(r)$	[66,67]
Electrophilic Parr function	$P^+(r) = \rho_s^{ra}(r)$	[66,67]

where $\rho_{N+1}(r)$, $\rho_N(r)$, and $\rho_{N-1}(r)$ are the electronic densities at point r for the system with N+1, N, and N−1 electrons, respectively, and $\rho_s^{rc}(r)$ and $\rho_s^{ra}(r)$ are related to the atomic spin density (ASD) at the r atom of the radical cation or anion of a given molecule, respectively [68].

Settings and Computational Methods

Following the lines of our previous work [3-33], the computational studies were performed with the Gaussian 09 [69] series of programs with density functional methods as implemented in the computational package. The basis set used in this work was Def2SVP for geometry optimization and frequencies, while Def2TZVP was considered for the calculation of the electronic properties [70, 71]. All the calculations were performed in the presence of water as the solvent by doing Integral Equation Formalism-Polarized Continuum Model (IEF-PCM) computations according to the solvation model density (SMD) solvation model [72].

For the calculation of the molecular structure and properties of the studied systems, we have chosen ten density functionals which are known to consistently provide satisfactory results for several structural and thermodynamic properties:

CAM-B3LYP	Long-range-corrected B3LYP by the CAM method	[73]
LC-ωPBE	Long-range-corrected ωPBE density functional	[74]
M11	Range-separated hybrid meta-GGA	[75]
M11L	Dual-range local meta-GGA	[76]
MN12L	Nonseparable local meta-NGA	[77]
MN12SX	Range-separated hybrid nonseparable meta-NGA	[78]
N12	Nonseparable local NGA	[79]
N12SX	Range-separated hybrid NGA	[78]
wB97X	Long-range corrected density functional	[80]
wB97XD	wB97X version including empirical dispersion	[81]

In these functionals, GGA stands for generalized gradient approximation (in which the density functional depends on the up and down spin densities and their reduced gradient) and NGA stands for non-separable gradient approximation (in which the density functional depends on the up/down spin densities and their reduced gradient, and also adopts a non-separable form).

Results and Discussion

The molecular structure of the seven key chromophores were built with the aid of a graphical molecular viewer starting from their IUPAC names. The pre-optimization of the systems was done using random sampling that involved molecular mechanics techniques and inclusion of the various torsional angles via the general MMFF94 force field [82-86] through the Marvin View 17.15 program that constitutes an advanced chemical viewer suited to multiple and single chemical queries, structures and reactions (https://www.chem axon.com). Afterwards, the structures that the resultant lower-energy conformers assumed for these molecules were re-optimized using the ten density functionals mentioned in the previous section together with the Def2SVP basis set as well as the SMD solvation model using water as the solvent. A graphical representation of these molecular structures is presented in [Figure 1].

The analysis of the results obtained in the study aimed at verifying that the KID procedure was fulfilled. On doing it previously, several descriptors associated with the results that HOMO and LUMO calculations obtained

are related with results obtained using the vertical I and A following the ΔSCF procedure. A link exists between the three main descriptors and the simplest conformity to the Koopmans' theorem by linking ε_H with -I, ε_L with -A, and their behavior in describing the HOMO-LUMO gap as $J_I = |\varepsilon_H + E_{gs}(N-1) - E_{gs}(N)|$, $J_A = |\varepsilon_L + E_{gs}(N) - E_{gs}(N+1)|$, and $J_{HL} = \sqrt{(J_I^2 + J_A^2)}$. Notably, the J_A descriptor consists of an approximation that remains valid only when the HOMO that a radical anion has (the SOMO) shares similarity with the LUMO that the neutral system has. Consequently, we decided to design another descriptor ΔSL, to guide in verifying how the approximation is accurate.

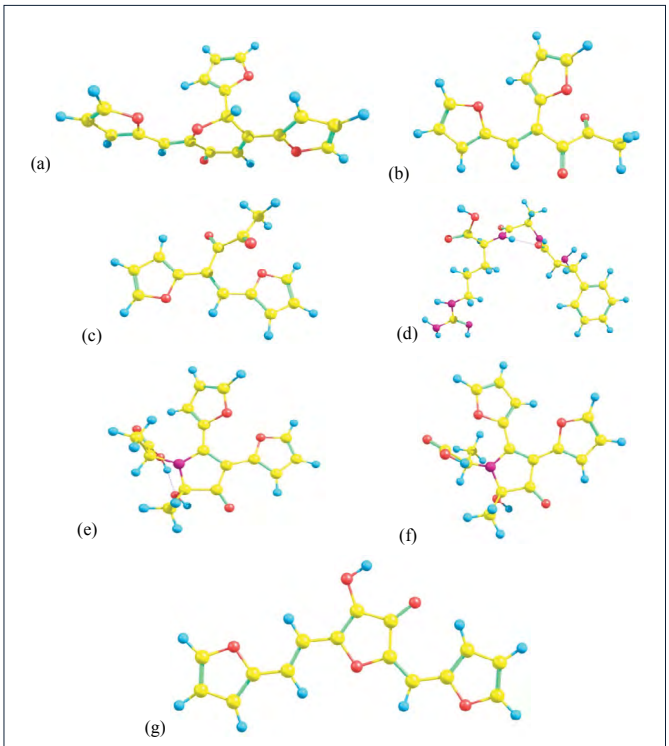

Figure 1: A graphical representation of the optimized molecular structures of the seven key chromophores: a) Key1, b) Key2a, c) Key2b, d) Key3, e) Key4a, f) Key4b, and g) Key5.

The results of the calculation of the electronic energies of the neutral, positive and negative molecular systems (in au) of PPA, the HOMO, LUMO and SOMO orbital energies (also in au), J_I, J_A, J_{HL} and ΔSL descriptors calculated with the ten density functionals and the Def2TZVP basis set using water as a solvent simulated with the SMD parametrization of the IEF-PCM model for the seven key chromophores are presented in [Tables 1 to 7] of the Supplementary Materials. As presented in previous works [3-33], we consider four other descriptors that analyze how well the studied density functionals are useful for the prediction of the electronegativity χ, the global hardness η, and the global electrophilicity ω, and for a combination of these Conceptual DFT descriptors, considering only the energies of the HOMO and LUMO or the vertical I and A: $J_\chi = |\chi-\chi_K|$, $J_\eta = |\eta-\eta_K|$, $J_\omega = |\omega-\omega_K|$, and $J_{CDFT} = \sqrt{(J_\chi^2+J_\eta^2+J_\omega^2)}$, where CDFT stands for Conceptual DFT. The results of the calculations of

	Eo	E+	E-	HOMO	LUMO	SOMO	J_I	J_A	J_{HL}	ΔSL
CAM-B3LYP	-1067.87	-1067.67	-1067.98	-0.261	-0.056	-0.156	0.053	0.050	0.073	0.100
LC-wPBE	-1067.66	-1067.45	-1067.78	-0.309	-0.026	-0.201	0.094	0.088	0.128	0.176
M11	-1067.79	-1067.57	-1067.90	-0.301	-0.032	-0.190	0.085	0.079	0.116	0.158
M11L	-1067.82	-1067.61	-1067.94	-0.207	-0.130	-0.113	0.010	0.009	0.013	0.018
MN12L	-1067.44	-1067.23	-1067.55	-0.197	-0.114	-0.099	0.009	0.008	0.012	0.015
MN12SX	-1067.47	-1067.25	-1067.58	-0.214	-0.111	-0.113	0.000	0.001	0.001	0.002
N12	-1067.38	-1067.19	-1067.48	-0.180	-0.110	-0.089	0.012	0.011	0.016	0.022
N12SX	-1067.93	-1067.73	-1068.04	-0.206	-0.105	-0.108	0.001	0.002	0.002	0.003
wB97X	-1068.11	-1067.90	-1068.22	-0.297	-0.026	-0.188	0.086	0.081	0.118	0.162
wB97XD	-1068.03	-1067.82	.1068.14	-0.283	-0.037	-0.177	0.073	0.070	0.101	0.140

Table 1: Electronic energies of the neutral, positive, and negative molecular systems (in au) of the Key1 chromophore, the HOMO, LUMO, and SOMO orbital energies (also in au); and J_I, J_A, J_{HL}, and ΔSL descriptors calculated with the ten density functionals and the Def2TZVP basis set using water as solvent simulated with the SMD parametrization of the IEF-PCM model.

	Eo	E+	E-	HOMO	LUMO	SOMO	J_I	J_A	J_{HL}	ΔSL
CAM-B3LYP	-801.267	-801.06	-801.37	-0.256	-0.055	-0.160	0.050	0.052	0.073	0.105
LC-wPBE	-801.110	-801.89	-801.22	-0.304	-0.022	-0.204	0.088	0.091	0.127	0.183
M11	-801.200	-801.98	-801.31	-0.296	-0.028	-0.193	0.080	0.083	0.115	0.165
M11L	-801.228	-801.02	-801.35	-0.204	-0.134	-0.113	0.009	0.010	0.014	0.021
MN12L	-800.927	-800.72	-801.04	-0.193	-0.118	-0.100	0.009	0.009	0.013	0.018
MN12SX	-800.952	-800.74	-801.06	-0.209	-0.112	-0.114	0.0001	0.001	0.001	0.002
N12	-801.617	-801.43	-801.72	-0.179	-0.117	-0.090	0.012	0.014	0.018	0.027
N12SX	-801.298	-801.10	-801.41	-0.202	-0.107	-0.110	0.001	0.001	0.002	0.003
wB97X	-801.442	-801.23	-801.55	-0.291	-0.023	-0.192	0.081	0.084	0.117	0.169
wB97XD	-801.384	-801.18	-801.49	-0.278	-0.036	-0.181	0.070	0.073	0.101	0.145

Table 2: Electronic energies of the neutral, positive, and negative molecular systems (in au) of the Key2a chromophore, the HOMO, LUMO, and SOMO orbital energies (also in au); and J_I, J_A, J_{HL}, and ΔSL descriptors calculated with the ten density functionals and the Def2TZVP basis set using water as solvent simulated with the SMD parametrization of the IEF-PCM model.

	Eo	E+	E-	HOMO	LUMO	SOMO	J_I	J_A	J_{HL}	ΔSL
CAM-B3LYP	-801.27	-801.07	-801.37	-0.251	-0.050	-0.156	0.049	0.053	0.073	0.107
LC-wPBE	-801.12	-801.90	-801.22	-0.298	-0.015	-0.201	0.087	0.092	0.127	0.187
M11	-801.20	-800.99	-801.31	-0.290	-0.022	-0.191	0.079	0.084	0.116	0.169
M11L	-801.23	-801.02	-801.35	-0.199	-0.133	-0.107	0.009	0.013	0.016	0.026
MN12L	-800.93	-800.73	-801.03	-0.189	-0.116	-0.093	0.009	0.012	0.015	0.023
MN12SX	-800.95	-800.75	-801.06	-0.205	-0.108	-0.108	0.001	0.000	0.001	0.000
N12	-801.62	-801.43	-801.72	-0.175	-0.117	-0.084	0.012	0.018	0.021	0.033
N12SX	-801.30	-801.10	-801.40	-0.197	-0.104	-0.104	0.001	0.000	0.001	0.000
wB97X	-801.44	-801.24	-801.55	-0.285	-0.017	-0.189	0.080	0.085	0.117	0.172
wB97XD	-801.39	-801.18	-801.49	-0.272	-0.031	-0.178	0.069	0.074	0.101	0.148

Table 3: Electronic energies of the neutral, positive, and negative molecular systems (in au) of the Key2b chromophore, the HOMO, LUMO, and SOMO orbital energies (also in au); and J_I, J_A, J_{HL}, and ΔSL descriptors calculated with the ten density functionals and the Def2TZVP basis set using water as solvent simulated with the SMD parametrization of the IEF-PCM model.

	Eo	E+	E-	HOMO	LUMO	SOMO	J_I	J_A	J_{HL}	ΔSL
CAM-B3LYP	-1330.69	-1330.47	-1330.71	-0.276	0.036	-0.078	0.060	0.056	0.082	0.114
LC-wPBE	-1330.51	-1330.28	-1330.53	-0.329	0.071	-0.126	0.105	0.098	0.144	0.197
M11	-1330.58	-1330.36	-1330.60	-0.319	0.064	-0.112	0.096	0.087	0.130	0.176
M11L	-1330.65	-1330.36	-1330.43	-0.204	-0.052	-0.038	0.091	0.274	0.288	0.014
MN12L	-1330.00	-1329.72	-1329.79	-0.199	-0.031	-0.019	0.084	0.245	0.259	0.012
MN12SX	-1330.11	-1329.89	-1330.14	-0.222	-0.025	-0.027	0.001	0.001	0.001	0.002
N12	-1331.13	-1330.93	-1330.94	-0.173	-0.038	-0.020	0.023	0.232	0.233	0.018
N12SX	-1330.69	-1330.48	-1330.71	-0.210	-0.019	-0.024	0.000	0.002	0.002	0.004
wB97X	-1331.02	-1330.80	-1331.04	-0.316	0.069	-0.113	0.096	0.090	0.132	0.182
wB97XD	-1330.93	-1330.72	-1330.95	-0.298	0.056	-0.100	0.080	0.078	0.111	0.156

Table 4: Electronic energies of the neutral, positive, and negative molecular systems (in au) of the Key3 chromophore, the HOMO, LUMO, and SOMO orbital energies (also in au); and J_I, J_A, J_{HL}, and ΔSL descriptors calculated with the ten density functionals and the Def2TZVP basis set using water as solvent simulated with the SMD parametrization of the IEF-PCM model.

	Eo	E+	E-	HOMO	LUMO	SOMO	J_I	J_A	J_{HL}	ΔSL
CAM-B3LYP	-1123.48	-1123.28	-1123.57	-0.245	-0.038	-0.143	0.051	0.053	0.074	0.105
LC-wPBE	-1123.27	-1123.07	-1123.37	-0.292	-0.006	-0.188	0.089	0.092	0.128	0.182
M11	-1123.40	-1123.20	-1123.50	-0.284	-0.012	-0.177	0.081	0.083	0.116	0.165
M11L	-1123.40	-1123.20	-1123.50	-0.192	-0.116	-0.093	0.010	0.011	0.015	0.022
MN12L	-1122.98	-1122.79	-1123.07	-0.182	-0.099	-0.080	0.009	0.010	0.013	0.019
MN12SX	-1123.02	-1122.83	-1123.12	-0.199	-0.094	-0.095	0.000	0.000	0.001	0.001
N12	-1123.89	-1123.71	-1123.97	0.167	-0.098	-0.072	0.012	0.014	0.018	0.026
N12SX	-1123.50	-1123.31	-1123.59	-0.191	-0.089	-0.092	0.001	0.002	0.002	0.003
wB97X	-1123.72	-1123.52	-1123.81	-0.280	-0.007	-0.175	0.083	0.085	0.118	0.168
wB97XD	-1123.64	-1123.45	-1123.74	-0.268	-0.019	-0.164	0.072	0.073	0.102	0.145

Table 5: Electronic energies of the neutral, positive, and negative molecular systems (in au) of the Key4a chromophore, the HOMO, LUMO, and SOMO orbital energies (also in au); and J_I, J_A, J_{HL}, and ΔSL descriptors calculated with the ten density functionals and the Def2TZVP basis set using water as solvent simulated with the SMD parametrization of the IEF-PCM model.

	Eo	E+	E-	HOMO	LUMO	SOMO	J_I	J_A	J_{HL}	ΔSL
CAM-B3LYP	-1123.48	-1123.28	-1123.57	-0.248	-0.042	-0.145	0.051	0.052	0.073	0.104
LC-wPBE	-1123.28	-1123.07	-1123.38	-0.295	-0.011	-0.190	0.089	0.091	0.127	0.180
M11	-1123.40	-1123.20	-1123.50	-0.287	-0.016	-0.179	0.081	0.082	0.115	0.163
M11L	-1123.40	-1123.20	-1123.51	-0.195	-0.118	-0.096	0.010	0.011	0.015	0.022
MN12L	-1122.98	-1122.79	-1123.08	-0.185	-0.102	-0.084	0.009	0.009	0.013	0.018
MN12SX	-1123.03	-1122.83	-1123.13	-0.202	-0.097	-0.098	0.000	0.000	0.001	0.001
N12	-1123.89	-1123.71	-1123.98	-0.171	-0.100	-0.075	0.012	0.013	0.018	0.025
N12SX	-1123.50	-1123.31	-1123.59	-0.194	-0.092	-0.095	0.001	0.002	0.002	0.003
wB97X	-1123.72	-1123.52	-1123.82	-0.283	-0.011	-0.177	0.082	0.084	0.118	0.167
wB97XD	-1123.64	-1123.45	-1123.74	-0.270	-0.022	-0.167	0.071	0.073	0.102	0.144

Table 6: Electronic energies of the neutral, positive, and negative molecular systems (in au) of the Key4b chromophore, the HOMO, LUMO, and SOMO orbital energies (also in au); and J_I, J_A, J_{HL}, and ΔSL descriptors calculated with the ten density functionals and the Def2TZVP basis set using water as solvent simulated with the SMD parametrization of the IEF-PCM model.

J_χ,J_η,J_ω and J_{CDFT} for the low-energy conformers of the seven key chromophores in water are displayed in [Tables 8] to 14 of the Supplementary Materials.

As [Tables 1 to 14] of the Supplementary Materials provide, the KID procedure applies accurately from MN12SX and N12SX density functionals that are range-separated hybrid meta-NGA as well as range-separated hybrid NGA density functionals respectively. In fact, the values of J_I, J_A, J_{HL} are actually not zero. Nevertheless, the results tend to be impressive especially for the MN12SX density functional. As well, the ΔSL descriptor reaches the minimum values when MN12SX and N12SX density functionals are used in the calculations. This implies that there are sufficient justifications to assume that the LUMO of the neutral approximates the electron affinity. The

	Eo	E+	E-	HOMO	LUMO	SOMO	J_I	J_A	J_{HL}	ΔSL
CAM-B3LYP	-952.52	-952.32	-952.63	-0.251	-0.067	-0.165	0.049	0.049	0.069	0.098
LC-wPBE	-952.31	-952.10	-952.44	-0.298	-0.039	-0.212	0.088	0.086	0.123	0.173
M11	-952.43	-952.22	-952.56	-0.290	0.045	-0.199	0.077	0.077	0.110	0.154
M11L	-952.46	-952.25	-952.59	-0.201	-0.136	-0.120	0.008	0.008	0.011	0.016
MN12L	-952.13	-951.93	-952.25	-0.191	-0.120	-0.107	0.006	0.006	0.010	0.013
MN12SX	-952.15	-951.95	-952.27	-0.207	-0.118	-0.120	0.001	0.001	0.001	0.002
N12	-952.94	-952.76	-953.05	-0.175	-0.115	-0.096	0.010	0.010	0.014	0.018
N12SX	-952.56	-952.36	-952.67	-0.199	-0.112	-0.116	0.002	0.002	0.003	0.004
wB97X	-952.71	-952.50	-952.83	-0.285	-0.039	-0.197	0.079	0.079	0.112	0.158
wB97XD	-952.64	-952.44	-952.76	-0.272	-0.048	-0.185	0.069	0.069	0.097	0.137

Table 7: Electronic energies of the neutral, positive, and negative molecular systems (in au) of the Key5 chromophore, the HOMO, LUMO, and SOMO orbital energies (also in au); and J_I, J_A, J_{HL}, and ΔSL descriptors calculated with the ten density functionals and the Def2TZVP basis set using water as solvent simulated with the SMD parametrization of the IEF-PCM model.

	$J\chi$	$J\eta$	$J\omega$	J_{CDFT}
CAM-B3LYP	0.0013	0.1029	0.0595	0.1189
LC-wPBE	0.0030	0.1813	0.0825	0.1992
M11	0.0029	0.1640	0.0754	0.1805
M11L	0.0006	0.0182	0.0345	0.0390
MN12L	0.0010	0.0169	0.0233	0.0288
MN12SX	0.0006	0.0006	0.0017	0.0019
N12	0.0005	0.0232	0.0368	0.0435
N12SX	0.0004	0.0029	0.0041	0.0050
wB97X	0.0026	0.1667	0.0729	0.1820
wB97XD	0.0017	0.1430	0.0701	0.1593

Table 8: $J\chi$, $J\eta$, $J\omega$ and J_{CDFT} for the Key1 chromophores in water.

	$J\chi$	$J\eta$	$J\omega$	J_{CDFT}
CAM-B3LYP	0.0011	0.1026	0.0641	0.1210
LC-wPBE	0.0017	0.1794	0.0846	0.1983
M11	0.0013	0.1628	0.0782	0.1806
M11L	0.0005	0.0196	0.0458	0.0499
MN12L	0.0001	0.0182	0.0313	0.0362
MN12SX	0.0007	0.0002	0.0014	0.0016
N12	0.0011	0.0255	0.0526	0.0584
N12SX	0.0003	0.0022	0.0035	0.0041
wB97X	0.0013	0.1655	0.0761	0.1822
wB97XD	0.0012	0.1431	0.0750	0.1616

Table 9: $J\chi$, $J\eta$, $J\omega$ and J_{CDFT} for the Key2a chromophore in water.

	$J\chi$	$J\eta$	$J\omega$	J_{CDFT}
CAM-B3LYP	0.0019	0.1026	0.0614	0.1196
LC-wPBE	0.0024	0.1795	0.0793	0.1962
M11	0.0025	0.1632	0.0746	0.1794
M11L	0.0018	0.0223	0.0553	0.0597
MN12L	0.0016	0.0210	0.0383	0.0437
MN12SX	0.0004	0.0007	0.0002	0.0009
N12	0.0030	0.0292	0.0664	0.0726
N12SX	0.0003	0.0009	0.0008	0.0012
wB97X	0.0025	0.1658	0.0724	0.1809
wB97XD	0.0023	0.1431	0.0725	0.1604

Table 10: $J\chi$, $J\eta$, $J\omega$ and J_{CDFT} for the Key2b chromophores in water.

	$J\chi$	$J\eta$	$J\omega$	J_{CDFT}
CAM-B3LYP	0.0017	0.1159	0.0126	0.1166
LC-wPBE	0.0038	0.2031	0.0191	0.2040
M11	0.0045	0.1834	0.0167	0.1842
M11L	0.0912	0.3647	0.0525	0.3796
MN12L	0.0806	0.3286	0.0380	0.3405
MN12SX	0.0008	0.0000	0.0005	0.0009
N12	0.1041	0.2550	0.0414	0.2785
N12SX	0.0012	0.0020	0.0011	0.0026
wB97X	0.0030	0.1861	0.0167	0.1869
wB97XD	0.0010	0.1571	0.0158	0.1579

Table 11: $J\chi$, $J\eta$, $J\omega$ and J_{CDFT} for the Key3 chromophores in water.

	$J\chi$	$J\eta$	$J\omega$	J_{CDFT}
CAM-B3LYP	0.0007	0.1040	0.0497	0.1153
LC-wPBE	0.0011	0.1808	0.0687	0.1934
M11	0.0008	0.1642	0.0625	0.1757
M11L	0.0003	0.0214	0.0342	0.0403
MN12L	0.0001	0.0188	0.0220	0.0289
MN12SX	0.0004	0.0000	0.0006	0.0007
N12	0.0007	0.0259	0.0352	0.0437
N12SX	0.0003	0.0027	0.0031	0.0041
wB97X	0.0009	0.1673	0.0607	0.1780
wB97XD	0.0008	0.1447	0.0583	0.1560

Table 12: $J\chi$, $J\eta$, $J\omega$ and J_{CDFT} for the Key4a chromophores in water.

	$J\chi$	$J\eta$	$J\omega$	J_{CDFT}
CAM-B3LYP	0.0007	0.1032	0.0517	0.1154
LC-wPBE	0.0009	0.1793	0.0715	0.1930
M11	0.0005	0.1631	0.0649	0.1755
M11L	0.0003	0.0206	0.0338	0.0396
MN12L	0.0000	0.0183	0.0221	0.0287
MN12SX	0.0004	0.0001	0.0006	0.0007
N12	0.0006	0.0249	0.0345	0.0425
N12SX	0.0004	0.0026	0.0032	0.0041
wB97X	0.0007	0.1662	0.0632	0.1778
wB97XD	0.0007	0.1438	0.0606	0.1561

Table 13: $J\chi$, $J\eta$, $J\omega$ and J_{CDFT} for the Key4b chromophore in water.

	$J\chi$	$J\eta$	$J\omega$	J_{CDFT}
CAM-B3LYP	0.0000	0.0982	0.0781	0.1255
LC-wPBE	0.0008	0.1742	0.1117	0.2069
M11	0.0010	0.1559	0.0974	0.1838
M11L	0.0000	0.0155	0.0415	0.0443
MN12L	0.0004	0.0137	0.0265	0.0298
MN12SX	0.0005	0.0008	0.0023	0.0025
N12	0.0003	0.0196	0.0423	0.0466
N12SX	0.0005	0.0034	0.0067	0.0075
wB97X	0.0004	0.1588	0.0954	0.1852
wB97XD	0.0000	0.1370	0.0904	0.1641

Table 14: $J\chi$, $J\eta$, $J\omega$ and J_{CDFT} for the Key5 chromophore in water.

same density functionals follow the KID procedure in the rest of the descriptors such as J_{χ},J_{η},J_{ω} and J_{CDFT}. As a summary of the previous results, the global reactivity descriptors for the seven key chromophores calculated with the MN12SX/Def2TZVP model chemistry in water are presented in [Table 15].

The calculations of are done by using the Chemcraft molecular analysis program to extract the Mulliken and NPA atomic charges [87] beginning with single-point energy calculations involving the MN12SX density functional that uses the Def2TZVP basis set in line with the SMD solvation model, and water utilized as the solvent. Considering the potential application of the key chromophores as antioxidants, it is of interest to get insight into the active sites for radical attack. A graphical representation of the radical Fukui function f^0 for the seven key chromophores calculated with the MN12SX/Def2TZVP model chemistry in water is presented in [Figure 2].

The condensed electrophilic and nucleophilic Parr functions P_k^- and P_k^+ over the atoms of the seven key chromophores in water have been calculated by extracting the Mulliken and Hirshfeld (or CM5) atomic charges using the Chemcraft molecular analysis program [87] starting from single-point energy calculations of the ionic species with the MN12SX density functional using the Def2TZVP basis set in the presence of the solvent according to the SMD solvation model. The results for the condensed dual descriptor calculated with Mulliken atomic charges $\Delta f_k(M)$, with NPA atomic charges $\Delta f_k(N)$, the electrophilic and nucleophilic Parr functions with Mulliken atomic charges $P_k^-(M)$ and $P_k^+(M)$, and the electrophilic and nucleophilic Parr functions with Hirshfeld (or CM5) atomic charges $P_k^-(H)$ and $P_k^+(H)$ are displayed in [Tables 16 to 22] for the seven key chromophores in water. The results from [Tables 16 to 22] show that the MN12SX/Def2TZVP/SMD(water) model chemistry is able to predict accurately the electrophilic and nucleophilic sites of the seven key chromophores studied here. Moreover, there is a nice match between the predictions coming from the Dual Descriptor and from the Parr functions.

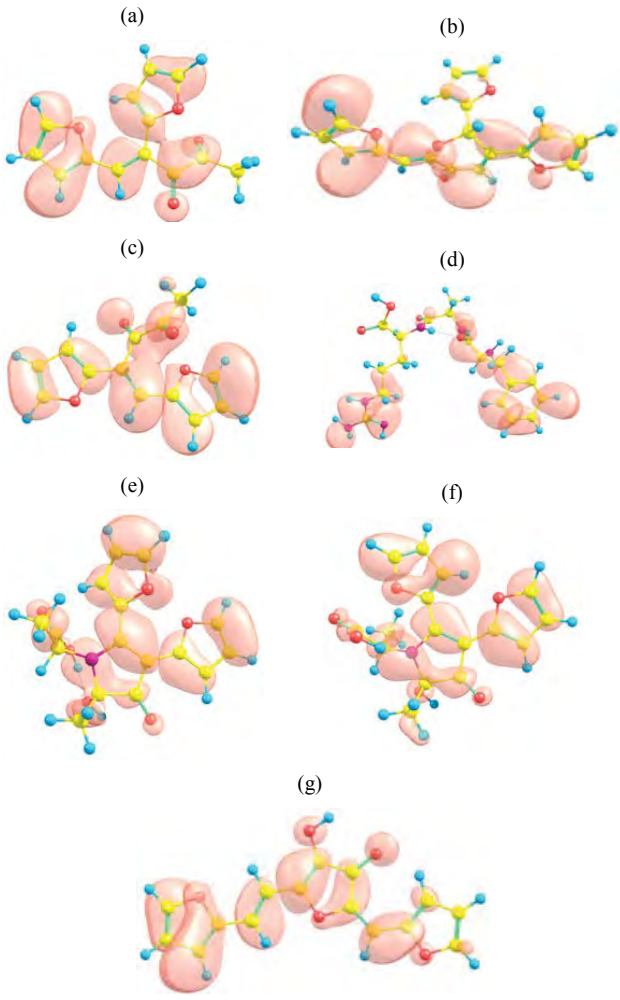

Figure 2: A graphical schematic representation of the radical Fukui function f^0 over the atomic sites of the seven key chromophores: a) Key1, b) Key2a, c) Key2b, d) Key3, e) Key4a, f) Key4b, and g) Key5.

	Electronegativity (χ)	**Chemical Hardness (η)**	**Electrophilicity (ω)**
Key1	4.4230	2.8108	3.4799
Key2a	4.3726	2.6503	3.6072
Key2b	4.2543	2.6203	3.4536
Key3	3.3591	5.3468	1.0522
Key4a	3.9863	2.8407	2.7969
Key4b	4.0665	2.8434	2.9079
Key5	4.4284	2.4190	4.0536
	Electrodonating Power (ω^-)	**Electroaccepting Power (ω^+)**	**Net Electrophilicity ($\Delta\omega^{\pm}$)**
Key1	5.4962	3.9892	9.4855
Key2a	5.6252	4.1448	9.7700
Key2b	5.4086	3.9652	9.3739
Key3	2.4250	1.0444	3.4694
Key4a	4.5656	3.1848	7.7505
Key4b	4.7199	3.3153	8.0351
Key5	6.1581	4.6783	10.8363

Table 15: Global reactivity descriptors for the seven key chromophores calculated with the MN12SX density functional using water as the solvent simulated with the SMD solvation model.

Atom	$\Delta f_k(M)$	$\Delta f_k(N)$	$P_k^+(M)$	$P_k^-(M)$	$P_k^+(H)$	$P_k^-(H)$
1C	15.61	10.70	0.2951	-0.0006	0.1554	0.0020
2C	3.59	1.06	-0.0512	0.0272	0.0276	0.0158
4C	15.79	13.37	0.2081	-0.0521	0.1550	0.0058
5O	11.16	7.92	0.2105	0.0532	0.1928	0.0436
6O	-6.60	-4.67	0.0093	0.0891	0.0091	0.0901
7C	-15.19	-13.55	-0.0296	0.2836	0.0267	0.1863
8C	0.42	0.37	-0.0255	-0.0117	0.0130	0.0058
10C	3.42	8.44	0.1656	-0.0086	0.0960	0.0539
12C	-0.21	1.37	-0.0851	0.0108	0.0011	0.0073
13C	7.66	7.09	0.1445	0.0054	0.0834	0.0053
14O	1.72	1.84	0.0211	-0.0014	0.0218	0.0001
15C	-0.22	-0.28	-0.0419	0.0015	-0.0043	0.0030
17C	5.07	4.89	0.1028	0.0146	0.0710	0.0111
20C	-0.37	0.73	0.0097	0.0220	0.0120	0.0132
21C	-0.30	0.38	-0.0008	0.0008	0.0017	0.0034
22O	-0.01	-0.12	0.0011	-0.0006	0.0019	0.0012
23C	0.06	0.00	0.0021	-0.0014	0.0012	0.0002
25C	-0.49	-0.19	-0.0008	0.0071	-0.0005	0.0051
28C	-14.49	-8.61	-0.0435	0.1878	-0.0001	0.1369
29C	-6.94	-4.58	0.0856	0.1407	0.0513	0.1240
30O	0.85	0.70	0.0133	-0.0341	0.0136	-0.0018
31C	-5.39	-4.46	-0.0255	0.0017	-0.0026	0.0435
33C	-15.35	-11.48	0.0633	0.2943	0.0438	0.2208

Table 16: The condensed dual descriptor calculated with Mulliken atomic charges $\Delta f_k(M)$, with NPA atomic charges $\Delta f_k(N)$, the nucleophilic and electrophilic Parr functions with Mulliken atomic charges $P_k^-(M)$ and $P_k^+(M)$, and the nucleophilic and electrophilic Parr functions with Hirshfeld (or CM5) atomic charges $P_k^-(H)$ and $P_k^+(H)$ for the Key1 chromophore in water.

Atom	$\Delta f_k(M)$	$\Delta f_k(N)$	$P_k^+(M)$	$P_k^-(M)$	$P_k^+(H)$	$P_k^-(H)$
1C	17.67	14.33	0.2129	-0.0302	0.1733	0.0057
2O	11.37	9.32	0.1993	0.0559	0.1849	0.0465
3C	-4.84	-4.48	-0.0162	0.1474	0.0411	0.1044
4C	12.80	10.68	0.3178	0.0275	0.1890	0.0526
6C	7.15	3.38	0.0438	0.0014	0.0559	0.0012
7O	5.09	6.15	0.0696	0.0005	0.0677	0.0007
8C	0.08	-0.08	-0.0071	0.0018	0.0056	0.0011
12C	-12.87	-6.60	-0.0038	0.1386	0.0067	0.1156
13C	-9.32	-5.96	0.0175	0.1465	0.0112	0.1200
14O	0.18	-0.43	0.0043	-0.0260	0.0094	0.0010
15C	-4.56	-3.37	-0.0061	-0.0102	-0.0007	0.0333
17C	-15.62	-11.44	0.0155	0.2577	0.0102	0.1916
20C	-6.64	-2.71	-0.0826	0.0856	0.0016	0.0675
21C	2.57	2.10	0.1683	0.0962	0.1019	0.0787
22O	1.68	1.91	0.0247	-0.0163	0.0258	0.0029
23C	-2.58	-2.30	-0.0511	-0.0048	-0.0050	0.0224
25C	-2.75	-2.11	0.1297	0.1711	0.0896	0.1277

Table 17: The condensed dual descriptor calculated with Mulliken atomic charges $\Delta f_k(M)$, with NPA atomic charges $\Delta f_k(N)$, the nucleophilic and electrophilic Parr functions with Mulliken atomic charges $P_k^-(M)$ and $P_k^+(M)$, and the nucleophilic and electrophilic Parr functions with Hirshfeld (or CM5) atomic charges $P_k^-(H)$ and $P_k^+(H)$ for the Key2a chromophore in water.

Atom	$\Delta f_k(M)$	$\Delta f_k(N)$	$P_k^+(M)$	$P_k^-(M)$	$P_k^+(H)$	$P_k^-(H)$
1C	9.33	4.59	0.1021	0.0011	0.0746	0.0013
2O	7.86	8.81	-0.4488	0.0019	0.0932	0.0024
3C	0.22	0.10	-0.0715	-0.0001	0.0046	0.0002
7C	23.85	18.58	0.0816	-0.0218	0.2020	0.0055
8O	17.35	13.78	-0.4996	0.0199	0.2282	0.0169
9C	-5.80	-6.68	-0.0934	0.1421	0.0397	0.0975
10C	6.02	6.02	-0.0863	0.0671	0.1486	0.0741
12C	-10.55	-5.79	0.1841	0.1026	0.0081	0.0962
13C	-9.69	-7.24	-0.1196	0.1515	0.0121	0.1213
14O	-0.13	-0.10	-0.4051	-0.0213	0.0020	0.0025
15C	-4.59	-3.35	-0.1275	-0.0074	-0.0009	0.0341
17C	-14.67	-10.90	0.1528	0.2519	0.0136	0.1883
20C	-7.24	-1.77	0.1472	0.0698	0.0041	0.0657
21C	-3.50	-1.77	-0.1178	0.1245	0.0631	0.0968
22O	1.28	0.20	-0.4087	-0.0166	0.0278	0.0010
23C	-2.83	-1.78	-0.1279	-0.0124	-0.0024	0.0221
25C	-7.90	-5.83	0.1445	0.1936	0.0549	0.1435

Table 18: The condensed dual descriptor calculated with Mulliken atomic charges $\Delta f_k(M)$, with NPA atomic charges $\Delta f_k(N)$, the nucleophilic and electrophilic Parr functions with Mulliken atomic charges $P_k^-(M)$ and $P_k^+(M)$, and the nucleophilic and electrophilic Parr functions with Hirshfeld (or CM5) atomic charges $P_k^-(H)$ and $P_k^+(H)$ for the Key2b chromophore in water.

Atom	$\Delta f_k(M)$	$\Delta f_k(N)$	$P_k^+(M)$	$P_k^-(M)$	$P_k^+(H)$	$P_k^-(H)$
1N	0.16	0.12	0.0047	0.0000	0.0049	0.0000
2C	1.56	0.06	0.0157	0.0000	0.0199	0.0000
3C	5.82	3.63	0.0622	0.0000	0.0486	0.0000
4O	2.31	2.54	0.0216	0.0000	0.0241	0.0000
5C	1.67	0.62	0.0046	0.0000	0.0210	0.0000
6C	11.11	6.26	0.1306	0.0000	0.1110	0.0000
7C	2.98	2.66	-0.0433	0.0000	0.0428	0.0000
8C	25.37	20.55	0.3708	0.0000	0.2260	0.0000
9C	11.07	8.19	0.0881	0.0000	0.0994	0.0000
10C	4.11	3.48	-0.0019	0.0000	0.0584	0.0000
11C	26.62	23.29	0.3825	0.0000	0.2295	0.0000
22N	1.58	1.18	0.0096	0.0001	0.0137	0.0001
23C	0.14	0.16	-0.0002	0.0001	0.0018	0.0000
24C	0.31	0.07	0.0023	-0.0003	0.0022	0.0001
25O	0.08	0.25	0.0012	0.0008	0.0012	0.0007
28C	0.02	0.04	0.0007	0.0000	0.0005	0.0000
32N	-0.04	0.16	0.0010	0.0017	0.0010	0.0013
33C	-0.08	-0.05	-0.0002	0.0004	0.0001	0.0007
34C	-0.01	-0.01	0.0000	0.0001	0.0000	0.0001
35O	-0.02	-0.01	0.0000	0.0001	0.0000	0.0001
36C	-0.27	-0.03	0.0007	0.0029	0.0002	0.0021
39C	-0.73	-0.37	0.0000	0.0086	0.0000	0.0101
42C	-1.41	-2.28	0.0000	-0.0136	0.0000	0.0269
45N	-30.20	-24.27	0.0000	0.3939	0.0000	0.2826
47C	-3.82	-2.80	0.0000	-0.1651	0.0000	0.0085
48N	-7.08	-7.89	0.0000	0.0583	0.0000	0.0361
51N	-51.22	-43.31	0.0000	0.7126	0.0000	0.5592
55O	0.00	-0.11	0.0000	0.0000	0.0001	0.0000

Table 19: The condensed dual descriptor calculated with Mulliken atomic charges $\Delta f_k(M)$, with NPA atomic charges $\Delta f_k(N)$, the nucleophilic and electrophilic Parr functions with Mulliken atomic charges $P_k^-(M)$ and $P_k^+(M)$, and the nucleophilic and electrophilic Parr functions with Hirshfeld (or CM5) atomic charges $P_k^-(H)$ and $P_k^+(H)$ for the Key3 chromophore in water.

Atom	Δf_k(M)	Δf_k(N)	P_k^+(M)	P_k^-(M)	P_k^+(H)	P_k^-(H)
1C	21.05	12.33	0.4423	-0.0231	0.2606	0.0328
2C	-11.57	-6.27	-0.0644	0.2537	0.0228	0.1536
3C	3.12	0.26	0.0244	-0.0162	0.0203	0.0052
4N	-4.26	-3.72	0.0618	0.1541	0.0770	0.1060
5C	10.08	9.37	0.1554	-0.0262	0.1239	0.0248
6O	4.05	3.38	0.1214	0.0908	0.1143	0.0761
7O	1.32	1.87	0.0145	0.0011	0.0232	0.0004
9C	0.81	0.28	0.0033	0.0031	0.0126	0.0011
13C	-0.04	0.05	0.0008	-0.0140	0.0056	0.0072
15C	-0.27	0.09	0.0029	0.0076	0.0044	0.0065
19C	-0.18	-0.08	0.0009	0.0093	0.0036	0.0067
20O	-0.36	-0.26	0.0010	0.0051	0.0011	0.0049
21O	-0.09	0.04	0.0017	0.0010	0.0015	0.0015
23C	-11.57	-5.48	0.0122	0.0838	0.0062	0.0983
24C	-12.76	-8.73	0.0018	0.1973	0.0018	0.1506
25O	-0.16	-0.28	0.0001	-0.0240	0.0007	0.0017
26C	-4.76	-3.33	-0.0016	-0.0224	-0.0001	0.0314
28C	-17.52	-12.42	0.0072	0.2858	0.0046	0.2120
31C	2.19	0.27	-0.1018	0.0194	0.0269	0.0141
32C	10.43	7.86	0.2107	0.0160	0.1180	0.0130
33O	3.37	3.08	0.0447	-0.0027	0.0491	0.0005
34C	-0.35	-0.47	-0.0627	0.0002	-0.0051	0.0048
36C	6.93	5.32	0.1453	0.0295	0.0995	0.0221

Table 20: The condensed dual descriptor calculated with Mulliken atomic charges Δf_k**(M)**, with NPA atomic charges Δf_k**(N),** the nucleophilic and electrophilic Parr functions with Mulliken atomic charges P_k^-**(M)** and P_k^+**(M)**, and the nucleophilic and electrophilic Parr functions with Hirshfeld (or CM5) atomic charges P_k^-**(H)** and P_k^+**(H)** for the Key4a chromophore in water.

Atom	Δf_k(M)	Δf_k(N)	P_k^+(M)	P_k^-(M)	P_k^+(H)	P_k^-(H)
1C	19.10	10.24	0.4367	-0.0074	0.2486	0.0399
2C	-9.18	-4.03	-0.0378	0.2371	0.0330	0.1455
3C	2.08	-0.02	0.0120	-0.0121	0.0153	0.0050
4N	-3.63	-3.04	0.0415	0.1191	0.0629	0.0845
5C	9.38	8.69	0.1364	-0.0255	0.1117	0.0229
6O	3.96	3.51	0.1121	0.0816	0.1051	0.0682
7O	0.96	1.47	0.0104	0.0010	0.0165	0.0006
9C	0.49	0.11	0.0029	0.0032	0.0103	0.0005
13C	0.01	0.15	0.0026	-0.0071	0.0069	0.0065
15C	-11.73	-5.96	0.0047	0.0910	0.0064	0.1004
16C	-11.82	-7.84	0.0145	0.1939	0.0092	0.1493
17O	0.01	-0.14	0.0019	-0.0241	0.0039	0.0023
18C	-4.76	-3.38	-0.0056	-0.0217	-0.0007	0.0318
20C	-16.97	-11.90	0.0158	0.2879	0.0105	0.2135
23C	1.04	-0.13	-0.1079	0.0249	0.0235	0.0192
24C	11.11	8.14	0.2309	0.0348	0.1367	0.0266
25O	3.32	2.72	0.0427	-0.0059	0.0465	-0.0005
26C	-0.47	-0.59	-0.0717	-0.0060	-0.0068	0.0046
28C	7.24	5.05	0.1773	0.0530	0.1206	0.0386
31C	-0.01	0.08	0.0038	0.0040	0.0030	0.0032
32O	-0.09	0.10	0.0010	0.0023	0.0013	0.0021
33O	-0.11	-0.03	0.0017	0.0022	0.0017	0.0025
35C	-0.17	-0.13	-0.0004	0.0086	0.0051	0.0058

Table 21: The condensed dual descriptor calculated with Mulliken atomic charges Δf_k**(M)**, with NPA atomic charges Δf_k**(N),** the nucleophilic and electrophilic Parr functions with Mulliken atomic charges P_k^-**(M)** and P_k^+**(M)**, and the nucleophilic and electrophilic Parr functions with Hirshfeld (or CM5) atomic charges P_k^-**(H)** and P_k^+**(H)** for the Key4b chromophore in water.

Atom	$\Delta f_k(M)$	$\Delta f_k(N)$	$P_k^+(M)$	$P_k^-(M)$	$P_k^+(H)$	$P_k^-(H)$
1C	-11.13	-10.96	-0.0693	0.1747	-0.0011	0.1208
2C	3.87	5.06	0.2054	0.0550	0.1216	0.0669
5C	-9.10	-4.23	-0.0553	0.1020	-0.0032	0.0862
6C	-3.95	-3.04	0.1044	0.1275	0.0623	0.1037
7O	0.64	0.47	0.0125	-0.0201	0.0132	0.0011
8C	-3.81	-3.07	-0.0301	-0.0038	-0.0028	0.0308
10C	-9.48	-7.36	0.0773	0.2194	0.0537	0.1643
13O	0.05	0.01	-0.0110	-0.0088	-0.0018	-0.0057
14C	5.61	7.28	0.1642	-0.0221	0.1039	0.0330
15C	-10.80	-10.35	-0.0473	0.2222	0.0061	0.1518
16O	-6.32	-5.19	-0.0010	0.0869	-0.0034	0.0874
18C	11.29	10.91	0.1648	-0.0322	0.1230	0.0099
19O	8.70	5.78	0.1736	0.0544	0.1582	0.0447
20C	1.63	0.19	-0.0495	0.0229	0.0192	0.0183
21C	15.65	11.89	0.2795	-0.0037	0.1605	0.0036
23C	-2.24	1.05	-0.0717	0.0236	-0.0020	0.0162
24C	5.44	5.54	0.1283	0.0153	0.0764	0.0141
25O	1.41	1.57	0.0185	-0.0040	0.0191	-0.0003
26C	-0.38	-0.30	-0.0371	-0.0021	-0.0032	0.0035
28C	2.91	3.34	0.0957	0.0323	0.0666	0.0238

Table 22: The condensed dual descriptor calculated with Mulliken atomic charges $\Delta f_k(M)$, with NPA atomic charges $\Delta f_k(N)$, the nucleophilic and electrophilic Parr functions with Mulliken atomic charges $P_k^-(M)$ and $P_k^+(M)$, and the nucleophilic and electrophilic Parr functions with Hirshfeld (or CM5) atomic charges $P_k^-(H)$ and $P_k^+(H)$ for the Key5 chromophore in water.

Conclusion

Ten fixed RSH density functionals, including CAM-B3LYP, LC-wPBE, M11, N12, M11L, MN12L, N12SX, MN12SX, wB97X and wB97XD, were examined to determine whether they fulfill the empirical KID procedure. The assessment was conducted by comparing the values from HOMO and LUMO calculations to those generated by the ΔSCF technique for the seven key chromophores derived from the reaction between hexoses an L-alanine in water. This is a compound which is of academic as well as industrial interest. The study has observed that the range-separated and hybrid meta-NGA density functionals tend to be the most suited in meeting this goal. Thus, they can be suitable alternatives to density functionals where the behavior of the same are optimally tuned using a gap-fitting procedure. They also exhibit the desirable prospect of benefiting future studies aimed at understanding the chemical reactivity of colored melanoidins with larger molecular weights when reducing sugars react with proteins and peptides. From the results of this work, it becomes evident that it is easy to predict the sites of interaction of the seven key chromophores under study. This involves having DFT-based reactivity descriptors, including Parr functions and Dual Descriptor calculations. Evidently, the descriptors are useful in characterizing and describing the preferred reactive sites. They are also useful in comprehensively explaining the reactivity of the molecules.

Acknowledgement

This work has been partially supported by CIMAV, SC and Consejo Nacional de Ciencia y Tecnología (CONACYT, Mexico) through Grant 219566-2014 for Basic Science Research. Daniel Glossman-Mitnik conducted this work while a Visiting Lecturer at the University of the Balearic Islands from which support is gratefully acknowledged. This work was cofunded by the Ministerio de Economía y Competitividad (MINECO) and the European Fund for Regional Development (FEDER) (CTQ2014-55835-R).

References

1. Rizzi GP (1997) Chemical Structure of Colored Maillard Reaction Products. *Food Reviews International* 13: 1-28. [View Article]

2. Frank O, Hofmann T (2000) Characterization of Key Chromophores Formed by Nonenzymatic Browning of Hexoses and L-Alanine by Using the Color Activity Concept. *J Agric Food Chem* 48: 6303-6311. [View Article]

3. Glossman Mitnik D (2013) A Comparison of the Chemical Reactivity of Naringenin Calculated with M06 Family of Density Functionals. *Chem Cent J* 7: 155-161. [View Article]

4. Salgado Morán G1, Ruiz Nieto S, Gerli Candia L, Flores Holguín N, Favila Pérez A, et al. (2013) Computational Nanochemistry Study of the Molecular Structure and Properties of Ethambutol. *J Mol Model* 19: 3507-3515. [View Article]

5. Martínez Araya JI, Salgado Morán G, Glossman Mitnik D (2013) Computational Nanochemistry Report on the Oxicams Conceptual DFT and Chemical Reactivity. *J Phys Chem B* 117: 6639-6651. [View Article]

6. Glossman Mitnik D (2013) Computational Nanochemistry Study of the Chemical Reactivity Properties of the Rhodamine B Molecule. *Procedia Computer Science* 18: 816-825. [View Article]

7. Martinez Araya JI, Salgado Moran G, Glossman Mitnik D (2013) Computational Nutraceutics: Chemical Reactivity Properties of the Flavonoid Naringin by Means of Conceptual DFT. *Journal of Chemistry* 2013: 1-8. [View Article]

8. Cervantes Navarro F, Glossman Mitnik D (2013) Density Functional Study of the Effects of Substituents on the Chemical Reactivity of the Indigo Molecule. *Journal of Theoretical and Computational Chemistry* 12: 1-12. [View Article]

9. Mónica Alvarado González, Norma Flores Holguín, Daniel Glossman Mitnik (2013) Computational Nanochemistry Study of the Molecular Structure and Properties of the Chlorophyll a Molecule. *International Journal of Photoenergy* 2013: 1-8. [View Article]

10. Glossman Mitnik D (2014) Chemical Reactivity Theory within DFT Applied to the Study of the Prunin Flavonoid. *European International Journal of Science and Technology* 3: 195-207. [View Article]

11. Glossman Mitnik D (2014) Computational Chemistry of Natural Products: A Comparison of the Chemical Reactivity of Isonaringin Calculated with the M06 Family of Density Functionals. *J Mol Model* 20: 2316. [View Article]

12. Glossman Mitnik D (2014) Computational Nanochemistry Study of the Molecular Structure, Spectra and Chemical Reactivity Properties of the BFPF Green Fluorescent Protein Chromophore. In: Tiwari A & Turner AP (Eds.), Biosensors Nanotechnology. *John Wiley & Sons*, Hoboken, USA, pp. 201-238. [View Article]

13. Glossman Mitnik D (2014) Computational Nanochemistry Report of the Molecular Structure, Spectra and Chemical Reactivity Properties of Pheophorbide A. In: Seminario JM (Ed.), Challenges and Advances in Computational Chemistry and Physics. *Design and Applications of Nanomaterials for Sensors*, Springer Science, Business Media, Dordrecht, Netherlands, pp. 217-247. [View Article]

14. Ignacio Martínez Araya, Grand A, Glossman Mitnik D (2015) Towards the Rationalization of Catalytic Activity Values by Means of Local Hyper-Softness on the Catalytic Site: A Criticism About the Use of Net Electric Charges. *Phys Chem Chem Phys* 17: 29764-29775. [View Article]

15. Soto Rojo R, Baldenebro López J, Glossman Mitnik D (2015) Study of Chemical Reactivity in Relation to Experimental Parameters of Efficiency in Coumarin Derivatives for Dye Sensitized Solar Cells Using DFT. *Phys Chem Chem Phys* 17: 14122-14129. [View Article]

16. Martinez Araya JI, Glossman Mitnik D (2015) The Substituent Effect from the Perspective of Local Hyper-Softness: An Example Applied on Normeloxicam, Meloxicam and 4-Meloxicam: Non-Steroidal Anti- Inflammatory Drugs. *Chemical Physics Letters* 618: 162-167. [View Article]

17. Frau J, Munoz F, Glossman Mitnik D (2016) Validation of the Koopmans' Theorem by Means of the Calculation of the Conceptual DFT Descriptors of Three Fluorescent DNA Staining Dyes. *Chemical Informatics* 2: 1-7. [View Article]

18. Frau J, Muñoz F, Glossman Mitnik D (2016) A Molecular Electron Density Theory Study of the Chemical Reactivity of cis- and trans-Resveratrol. *Molecules* 21: 1650. [View Article]

19. Frau J, Muñoz F, Glossman Mitnik D (2016) A Theoretical Study of the Chemical Reactivity of Neohesperidin Dihydrochalcone Through Conceptual DFT Descriptors. *SDRP Journal of Computational Chemistry and Molecular Modeling* 1:1-3. [View Article]

20. Mendoza Huizar LH, Salgado Morán G, Ramirez Tagle R, Glossman Mitnik D (2016) A Theoretical Quantum Study of the Intramolecular Interactions and Chemical Reactivity of Polymorphs A and B of Famotidine in the Gas, DMSO, and Aqueous Phases. *Computational and Theoretical Chemistry* 1075: 54-62. [View Article]

21. Frau J, Muñoz F, Glossman Mitnik D (2017) A Comparison of the Minnesota Family of Density Functionals for the Calculation of Conceptual DFT Descriptors: Citrus Flavonoids as a Test Case. *Research Journal of Chemical Sciences* 7: 46-58. [View Article]

22. Frau J, Glossman Mitnik D (2017) A Comparative Study of the Glycating Power of Simple Carbohydrates in the Maillard Reaction by Means of Conceptual DFT Descriptors. *British Journal of Applied Science and Technology* 21: 1-12. [View Article]

23. Frau J, Muñoz F, Glossman Mitnik D (2017) A Conceptual DFT Study of the Chemical Reactivity of Magnesium Octaethylprphyrin (MgOEP) as Predicted by the Minnesota Family of Density Functionals. *Quim Nova* 40: 402-406. [View Article]

24. Frau J, Glossman Mitnik D (2017) Pyridoxamine Derivatives as Non Enzymatic Glycation Inhibitors: The Conceptual DFT Viewpoint. *Research Journal of Life Sciences, Bioinformatics, Pharmaceutical and Chemical Sciences* 2: 103-122. [View Article]

25. Frau J, Glossman Mitnik D (2017) Molecular Modeling Study of the Structures, Properties and Glycating Power of Some Reducing Disacharides. *MOJ Drug Design Development & Therapy* 1: 1-14. [View Article]

26. Frau J, Glossman Mitnik D (2017) Computational Prediction of the Reactivity sites of Alzheimer Amyloid β-Peptides Aβ40 and Aβ42. *ChemXpress* 10: 1-7. [View Article]

27. Frau J, Glossman Mitnik D (2017) Conceptual DFT Descriptors of Amino Acids with Potential Corrosion Inhibition Properties Calculated with the Latest Minnesota Density Functionals. *Front Chem* 5: 1-16. [View Article]

28. Sastre S, Frau J, Glossman Mitnik D (2017) Computational Prediction of the Protonation Sites of Ac-Lys-(Ala)n-Lys-NH2 Peptides through Conceptual DFT and MEDT Descriptors. *Molecules* 22: 458. [View Article]

29. Frau J, Ramis R, Glossman Mitnik D (2017) Computational Prediction of the Preferred Glycation Sites of Model Helical Peptides Derived from Human Serum Albumin (HSA) and Lysozyme Helix 4 (LH4). *Theoretical Chemistry Accounts* 136: 1-39. [View Article]

30. Frau J, Muñoz F, Glossman Mitnik D (2017) Application of DFT Concepts to the Study of the Chemical Reactivity of Some Resveratrol Derivatives Through the Assessment of the Validity of the Koopmans in DFT (KID) Procedure. *Journal of Theoretical and Computational Chemistry* 16: 1750006. [View Article]

31. Frau J, Glossman Mitnik D (2017) Chemical Reactivity Theory Study of Advanced Glycation Endproduct Inhibitors. *Molecules* 22: 226. [View Article]

32. Frau J, Glossman Mitnik D (2017) A Conceptual DFT Study of the Molecular Properties of Glycating Carbonyl Compounds. *Chem Cent* J 11: 8. [View Article]

33. Frau J, Hernandez Haro N, Glossman Mitnik D (2017) Computational Prediction of the pKas of Small Peptides through Conceptual DFT Descriptors. *Chemical Physics Letters* 671: 138-141. [View Article]

34. Jacquemin D, Moore B, Planchat A, Adamo C, Autschbach J (2014) Performance of an Optimally Tuned Range-Separated Hybrid Functional for 0-0 Electronic Excitation Energies. *J Chem Theory Comput* 10: 1677-1685. [View Article]

35.Egger DA, Weissman S, Refaely Abramson S, Sharifzadeh S, Dauth M, et al. (2014) Outer-Valence Electron Spectra of Prototypical Aromatic Heterocycles From an Optimally Tuned Range-Separated Hybrid Functional. *J Chem Theory Comput* 10: 1934-1952. [View Article]

36.Foster ME, Wong BM (2012) Nonempirically Tuned Range-Separated DFT Accurately Predicts Both Fundamental and Excitation Gaps in DNA and RNA Nucleobases. *J Chem Theory Comput* 8: 2682-2687. [View Article]

37.Foster ME, Azoulay JE, Wong BM, Allendorf MD (2014) Novel Metal-Organic Framework Linkers for Light Harvesting Applications. *Chemical Science* 5: 2081-2090. [View Article]

38.Karolewski A, Stein T, Baer R, Kummel S (2011) Communication: Tailoring the Optical Gap in Light-Harvesting Molecules. *J Chem Phys* 134: 151101-151105. [View Article]

39.Karolewski A, Kronik L, Kummel S (2013) Using Optimally Tuned Range Separated Hybrid Functionals in Ground-State Calculations: Consequences and Caveats. *J Chem Phys* 138: 204115. [View Article]

40.Koppen JV, Hapka M, Szczeniak MM, Chalasinski G (2012) Optical Absorption Spectra of Gold Clusters Au(n) (n = 4, 6, 8,12, 20) From Long Range Corrected Functionals with Optimal Tuning. *J Chem Phys* 137: 114302. [View Article]

41.Kronik L, Stein T, Refaely Abramson S, Baer R (2012) Excitation Gaps of Finite-Sized Systems from Optimally Tuned Range-Separated Hybrid Functionals. *J Chem Theory Comput* 8: 1515-1531. [View Article]

42.Kuritz N, Stein T, Baer R, Kronik L (2011) Charge-Transfer-Like $\pi \rightarrow \pi^*$ Excitations in Time-Dependent Density Functional Theory: A Conundrum and Its Solution. *Journal of Chemical Theory and Computation* 7: 2408-2415. [View Article]

43.Lima IT, Prado ADS, Martins JBS, Ceschin AM, Da Cunha WF, et al. (2016) Improving the Description of the Optical Properties of Carotenoids by Tuning the Long-Range Corrected Functionals. *The J Phys Chem A* 120: 4944-4950. [View Article]

44.Manna Ak, Lee MH, McMahon KL, Dunietz BD (2015) Calculating High Energy Charge Transfer States Using Optimally Tuned Range- Separated Hybrid Functionals. *J Chem Theory Comput* 11: 1110-1117. [View Article]

45.Moore B, Autschbach J (2013) Longest Wavelength Electronic Excitations of Linear Cyanines: The Role of Electron Delocalization and of Approximations in Time-Dependent Density Functional Theory. *Journal of Chemical Theory and Computation* 9: 4991-5003. [View Article]

46.Niskanen M, Hukka TI (2014) Modeling of Photoactive Conjugated Donor- Acceptor Copolymers: the Effect of the Exact HF Exchange in DFT Functionals on Geometries and Gap Energies of Oligomer and Periodic Models. *Phys Chem Chem Phys* 16: 13294-13305. [View Article]

47.Pereira TL, Leal LA, Da Cunha WF, Timoteo de Sousa Junior R, Ribeiro Junior LA, et al. (2017) Optimally Tuned Functionals Improving the Description of Optical and Electronic Properties of the Phthalocyanine Molecule. *J Mol Model* 23: 71. [View Article]

48.Phillips H, Zheng S, Hyla A, Laine R, Goodson T, et al. (2012) Ab Initio Calculation of the Electronic Absorption of Functionalized Octahedral Silsesquioxanes via Time-Dependent Density Functional Theory with Range-Separated Hybrid Functionals. *J Phys Chem* A 116: 1137-1145. [View Article]

49.Phillips H, Geva E, Dunietz BD (2012) Calculating Off-Site Excitations in Symmetric Donor-Acceptor Systems via Time-Dependent Density Functional Theory with Range-Separated Density Functionals. *Journal of Chemical Theory and Computation* 8: 2661-2668. [View Article]

50.Refaely Abramson S, Baer R, Kronik L (2011) Fundamental and Excitation Gaps in Molecules of Relevance for Organic Photovoltaics From an Optimally Tuned Range-Separated Hybrid Functional. *Physical Review* B 84: 0751441-0751448. [View Article]

51.Stein T, Kronik L, Baer R (2009) Prediction of Charge-Transfer Excitations in Coumarin-Based Dyes Using a Range-Separated Functional Tuned From First Principles. *J Chem Phys* 131: 244119. [View Article]

52.Stein T, Kronik L, Baer R (2009) Reliable Prediction of Charge Transfer Excitations in Molecular Complexes Using Time-Dependent Density Functional Theory. *J Am Chem Soc* 131: 2818-2820. [View Article]

53.Sun H, Autschbach J (2014) Electronic Energy Gaps for π-Conjugated Oligomers and Polymers Calculated with Density Functional Theory. *J Chem Theory Comput* 10: 1035-1047. [View Article]

54.Parr R, Yang W (1984) Density Functional Approach to the Frontier-Electron Theory of Chemical Reactivity. *Journal of the American Chemical Society* 106: 4049-4050. [View Article]

55.Geerlings P, De Proft F, Langenaeker W (2003) Conceptual Density Functional Theory. *Chem Rev* 103: 1793-1873. [View Article]

56.Parr R, Szentpaly L, Liu S (1999) Electrophilicity Index. *Journal of the American Chemical Society* 121: 1922-1924. [View Article]

57.Gazquez J, Cedillo A, Vela A (2007) Electrodonating and Electroaccepting Powers. *J Phys Chem A* 111: 1966-1970. [View Article]

58.Chattaraj P, Chakraborty A, Giri S (2009) Net Electrophilicity. *J Phys Chem A* 113: 10068-10074. [View Article]

59.Morell C, Grand A, Toro Labbe A (2005) New Dual Descriptor for Chemical Reactivity. *J Phys Chem A* 109: 205-212. [View Article]

60.Morell C, Grand A, Toro Labbe A (2006) Theoretical Support for using the Δf(r) Descriptor. *Chemical Physics Letters* 425: 342-346. [View Article]

61.Cardenas C, Rabi N, Ayers P, Morell C, Jaramillo P, et al. (2009) Chemical Reactivity Descriptors for Ambiphilic Reagents: Dual Descriptor, Local Hypersoftness, and Electrostatic Potential. *J Phys Chem A* 113: 8660-8667. [View Article]

62.Toro Labbe A (2007) Theoretical Aspects of Chemical Reactivity. *Elsevier*, Amsterdam, USA, pp. 1-330. [View Article]

63.Ayers P, Morell C, De Proft F, Geerlings P (2007) Understanding the Woodward-Hoffmann Rules by Using Changes in Electron Density. *Chemistry - A European Journal* 13: 8240-8247. [View Article]

64.Morell C, Ayers P, Grand A, Gutierrez Oliva S, Toro Labbe A (2008) Rationalization of the Diels-Alder Reactions through the Use of the Dual Reactivity Descriptor Δf(r). *Physical Chemistry Chemical Physics* 10: 7239-7246. [View Article]

65.Morell C, Hocquet A, Grand A, Jamart Gregoire B (2008) A Conceptual DFT Study of Hydrazino peptides: Assessment of the Nucleophilicity of the Nitrogen Atoms by Means of the Dual

Descriptor Δf(r). *Journal of Molecular Structure: Theochem* 849: 46-51. [View Article]

66. Domingo LR, Perez P, Saez J (2013) Understanding the Local Reactivity in Polar Organic Reactions through Electrophilic and Nucleophilic Parr Functions. *RSC Advances* 3: 1486-1494. [View Article]

67. Chamorro E, Perez P, Domingo LR (2013) On the Nature of Parr Functions to Predict the Most Reactive Sites along Organic Polar Reactions. *Chemical Physics Letters* 582: 141-143. [View Article]

68. Domingo LR, Rios Gutierrez M, Perez P (2016) Applications of the Conceptual Density Functional Theory Indices to Organic Chemistry Reactivity. *Molecules* 21: 748. [View Article]

69. Frisch MJ, Trucks GW, Schlegel HB, Scuseria GE, Robb MA, et al. (2009) Gaussian 09 Revision D.01. Gaussian Inc., *The Royal Society of Chemistry*, Wallingford CT, USA, p. 1-20. [View Article]

70. Weigend F, Ahlrichs R (2005) Balanced Basis Sets of Split Valence, Triple Zeta Valence and Quadruple Zeta Valence Quality for H to Rn: Design and Assessment of Accuracy. *Phys Chem Chem Phys* 7: 3297-3305. [View Article]

71. Weigend F (2006) Accurate Coulomb-fitting Basis Sets for H to R. *Phys Chem Chem Phys* 8: 1057-1065. [View Article]

72. Marenich A, Cramer C, Truhlar D (2009) Universal Solvation Model Based on Solute Electron Density and a Continuum Model of the Solvent Defined by the Bulk Dielectric Constant and Atomic Surface Tensions. *J Phys Chem B* 113: 6378-6396. [View Article]

73. Yanai T, Tew DP, Handy NC (2004) A New Hybrid Exchange-Correlation Functional Using the Coulomb-Attenuating Method (CAM-B3LYP). *Chemical Physics Letters* 393: 51-57. [View Article]

74. Henderson TM, Izmaylov AF, Scalmani G, Scuseria GE (2009) Can Short-Range Hybrids Describe Long-Range-Dependent Properties? *The Journal of Chemical Physics* 131: 044108. [View Article]

75. Peverati R, Truhlar DG (2011) Improving the Accuracy of Hybrid Meta- GGA Density Functionals by Range Separation. *J Phys Chem Lett* 2: 2810-2817. [View Article]

76. Peverati R, Truhlar DG (2012) M11-L: A Local Density Functional That Provides Improved Accuracy for Electronic Structure Calculations in Chemistry and Physics. *J Phys Chem Lett* 3: 117-124. [View Article]

77. Peverati R, Truhlar DG (2012) An Improved and Broadly Accurate Local Approximation to the Exchange-Correlation Density Functional: the MN12-L Functional for Electronic Structure Calculations in Chemistry and Physics. *Physical Chemistry Chemical Physics* 14: 13171-13174. [View Article]

78. Peverati R, Truhlar DG (2012) Screened-Exchange Density Functionals with Broad Accuracy for Chemistry and Solid-State Physics. *Phys Chem Chem Phys* 14: 16187-16191. [View Article]

79. Peverati R, Truhlar DG (2012) Exchange-Correlation Functional with Good Accuracy for Both Structural and Energetic Properties while Depending Only on the Density and Its Gradient. *J Chem Theory Comput* 8: 2310-2319. [View Article]

80. Chai J, Head Gordon M (2008) Systematic Optimization of Long-Range Corrected Hybrid Density Functionals. *Journal of Chemical Physics* 128: 084106. [View Article]

81. Chai J, Head Gordon M (2008) Long-Range Corrected Hybrid Density Functionals with Damped Atom-Atom Dispersion Corrections. *Phys Chem Chem Phys* 10: 6615-6620. [View Article]

82. Halgren TA (1996) Merck Molecular Force Field. I. Basis, Form, Scope, Parameterization, and Performance of MMFF94. *Journal of Computational Chemistry* 17: 490-519. [View Article]

83. Halgren TA (1996) Merck Molecular Force Field. II. MMFF94 van der Waals and Electrostatic Parameters for Intermolecular Interactions. *Journal of Computational Chemistry* 17: 520-552. [View Article]

84. Halgren TA (1999) MMFF VI. MMFF94s Option for Energy Minimization Studies. *Journal of Computational Chemistry* 20: 720-729. [View Article]

85. Halgren TA, Nachbar RB (1996) Merck Molecular Force Field. IV. Conformational Energies and Geometries for MMFF94. *Journal of Computational Chemistry* 17: 587-615. [View Article]

86. Halgren TA (1996) Merck Molecular Force field. V. Extension of MMFF94 Using Experimental Data, Additional Computational Data, and Empirical Rules. *Journal of Computational Chemistry* 17: 616-641. [View Article]

87. Zhurko G, Zhurko D (2012) Chemcraft program Revision 1.6. In: Grigoriy Zhurko A (Eds.), USA. [View Article]

Citation: Glossman-Mitnik D, Frau J (2018) Molecular Reactivity of some Maillard Reaction Products Studied through Conceptual DFT. Contemp Chem 1: 001-014.